Inorganic Chemistry

Article

pubs.acs.org/IC

New Kagome Metal $Sc_3Mn_3Al_7Si_5$ and Its Gallium-Doped Analogues: Synthesis, Crystal Structure, and Physical Properties

Hua He,*[,†] Wojciech Miiller,[†] and Meigan C. Aronson[†,‡]

[†]Department of Physics and Astronomy, Stony Brook University, Stony Brook, New York 11794, United States

[‡]Condensed Matter Physics and Materials Science Department, Brookhaven National Laboratory, Upton, New York 11973, United States

Supporting Information

ABSTRACT: We report the synthesis, crystal structure, and basic properties of the new intermetallic compound $Sc_3Mn_3Al_7Si_5$. The structure of the compound was established by single-crystal X-ray diffraction, and it crystallizes with a hexagonal structure ($Sc_3Ni_{11}Si_4$ type) with Mn atoms forming the Kagome nets. The dc magnetic susceptibility measurements reveal a Curie–Weiss moment of ~0.51 μ_B/Mn; however, no magnetic order is found for temperatures as low as 1.8 K. Electrical resistivity and heat capacity measurements show that this compound is definitively metallic, with a relatively large specific heat Sommerfeld coefficient, indicating strong electronic correlations. Intriguingly, these features have revealed $Sc_3Mn_3Al_7Si_5$ as a possible quantum spin liquid. With chemical and lattice disorder introduced by doping, a spin liquid to spin glass transition is observed in the highest Ga-doped compounds. The roles of the geometrically frustrated structure and Mn-ligand hybridization in the magnetism of the title compounds are also discussed.

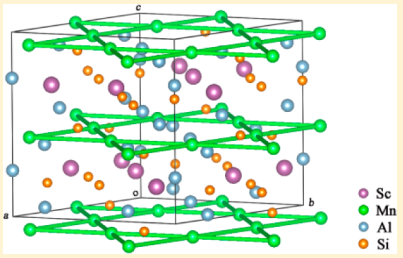

INTRODUCTION

Geometrically frustrated magnetic (GFM) materials have attracted much interest due to their unusual magnetic properties.[1−3] A triangle of antiferromagnetically interacting spins is the simplest example of geometrical frustration. Antiparallel coupling among all three spins cannot be satisfied simultaneously. This results in degenerate ground states, and the system fluctuates among all the possible spin configurations. Long-range magnetic order is suppressed by fluctuations among these configurations, leading to the formation of exotic magnetic ground states, like spin glass,[4] spin ice,[5] and spin liquid.[1,6] Common to each of these states is the absence of long-range order, although the presence of pronounced spatial and temporal correlations among the moments also makes them different from simple paramagnets, where the moments are noninteracting. In a spin glass, the magnetically disordered state is due to competing antiferromagnetic and ferromagnetic interacting spins,[4] while the spin ice states are usually found in particular frustrated lattices, as in the pyrochlore-type materials,[5] where the local spin configurations follow the so-called "ice rules".[7] Spin liquid is a more generic term referring to a highly correlated state that has no static order, where the fluctuations of the spins could be classical or quantum, i.e., quantum spin liquid (QSL) if the spins do not order or freeze down to the zero temperature.[1,6] The experimental realization of QSL has been a long-sought goal not just because it represents a novel state of matter but also due to its connections to the superconducting state in the cuprates proposed by Anderson.[6,8,9]

The Kagome net, one of the archetypes of GFM systems, is formed by corner-shared triangles of magnetic ions. Most Kagome compounds under study are insulating. They are ionic or metal–organic compounds in which the magnetic moments have a highly localized character, e.g., $YCa_3(VO)_3(BO_3)_4$,[10] $Cu_3Mg(OH)_6Cl_2$,[11] and $ZnCu_3(OD)_6Cl_2$.[12,13] Strong magnetic frustration was revealed in these compounds, and exotic ground states were proposed for them. More excitement was brought by $ZnCu_3(OD)_6Cl_2$, when fractional spin excitations, a hallmark of the quantum spin liquid state, have been observed.[13]

On the other hand, the physics of magnetic frustration and spin liquid in metallic systems is relatively unexplored, largely due to a lack of model systems. For instance, in the well-explored RMn_6X_6 (R = rare earth ion, X = Sn, Ge) family[14] with Mn Kagome nets, all members order magnetically with relatively high transition temperatures. Magnetic frustration suppresses magnetic order via competing interactions, and so conversely the observation of magnetic order at high temperatures implies that frustration is ineffectual in these compounds. $LaRu_3Si_2$ also contains Kagome nets, formed by the 4d transition metal Ru. While it is possible that electronic correlations exist in this compound, this system has no significant magnetic character.[15,16] The possible formation of a metallic spin liquid state has been revealed in a few GFM systems other than Kagome nets, e.g., β-Mn,[17] the pyrochlore-type $Y(Sc)Mn_2$,[18] and In-doped YMn_2Zn_{20}.[19] All these systems exhibit strong electronic correlations related to the presence of significant quantum spin fluctuations.[20,21]

In this article we report a new manganese-based intermetallic compound, $Sc_3Mn_3Al_7Si_5$, in which the Mn atoms form

Received: May 14, 2014
Published: August 21, 2014

   dx.doi.org/10.1021/ic501088t | Inorg. Chem. 2014, 53, 9115–9121

Kagome nets. Our magnetic and electronic property studies show that this material behaves like an itinerant spin liquid, with no magnetic order above 1.8 K. Low values of the effective Mn moment, an enhanced Sommerfeld coefficient, and a metallic temperature dependence of the electrical resistivity are consistent with the predominantly band character of magnetism in this compound, suggesting $Sc_3Mn_3Al_7Si_5$ is a rare example of a frustrated system where the spin liquid state involves itinerant electrons. We also show that by introducing Ga-doping, a spin liquid to spin glass transition is observed in the Ga-doped $Sc_3Mn_3Al_7Si_5$. These intriguing physical properties are discussed in the context of its GFM structure and complex chemical bonding.

EXPERIMENTAL SECTION

Single crystals of $Sc_3Mn_3Al_7Si_5$ were grown from a reactive aluminum flux. The elements Sc/Mn/Al/Si with a molar ratio 3:3:30:5 were loaded into an alumina crucible, which was then placed into a fused silica tube and sealed under high purity argon. The reaction vessel was heated to 1100 °C, maintained at that temperature for 8 h, and subsequently cooled to 750 °C during a period of 70 h. The molten Al flux was removed with a centrifuge at 750 °C. Bar-shaped crystals with dimensions as large as 6−8 mm were observed upon opening the silica tube (inset, Figure 1). Ga-doped crystals were grown from mixtures of

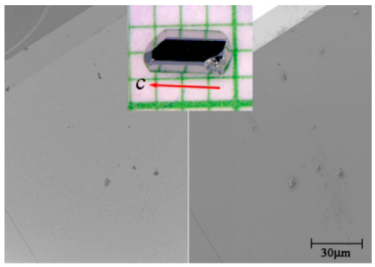

Figure 1. BSE (left) and SE (right) images of a crystal of $Sc_3Mn_3Al_7Si_5$, showing that the crystal is homogeneous. On top is a photo of the ~3 mm × 2 mm × 2 mm crystal under an optical microscope.

Al/Ga as reactive fluxes. As the Ga concentration in the mixture increased, the amount of Ga included in the final composition increased as well. For example, a mixture with 33% Ga was employed to make the 15% Ga-doped crystals, and the 19% Ga-doped crystals were actually made from a Ga:Al = 50%:50% flux. Further increasing the Ga:Al to 66.7%:33.3% produced only crystals of a different phase: $ScMnSi_2$.[22]

The crystal structures of $Sc_3Mn_3Al_7Si_5$ and its Ga-doped analogues were established by single-crystal X-ray diffraction. The intensity data were collected at room temperature using a Bruker KAPPA APEX II diffractometer with Mo $K\alpha$ radiation (λ = 0.710 73 Å). Data integration/reduction and an absorption correction with a multiscan method were performed with the Bruker APEX2 software suite. The structure was solved by the direct method and refined by a full matrix least-squares method against F^2 using the SHELX package.[23] The crystallographic data and the refinement parameters of $Sc_3Mn_3Al_7Si_5$ are summarized in Table 1. The atomic coordinates and equivalent isotropic displacement parameters, as well as important interatomic distances, are tabulated in Table 2 and Table 3, respectively. Further details of the crystal structure investigation, including the CIF file, can be obtained from the Supporting Information. The CIF file of $Sc_3Mn_3Al_7Si_5$ was also deposited in Fachinformationszentrum Karlsruhe, 76344 Eggenstein-Leopoldshafen, Germany (fax: (49)7247-808-666; e-mail: crysdata@fiz.karlsruhe.de) with depository number CSD-426711.

Several details about the structural determination of $Sc_3Mn_3Al_7Si_5$ need to be noted. Since Al and Si have similar scattering form factors,

Table 1. Refinement Parameters and Crystallographic Data of Single-Crystal X-ray Diffraction of $Sc_3Mn_3Al_7Si_5$

empirical formula	$Sc_3Mn_3Al_7Si_5$
fw	629.01
temperature (K)	299(2)
λ (Å)	0.71073
space group, Z	$P6_3/mmc$ (no. 194), 2
a (Å)	8.3519(2)
c (Å)	9.0845(4)
V (Å^3)	548.78(3)
ρ_{calcd} (g/cm^3)	3.807
goodness-of-fit	1.085
R_1 [$I > 2\sigma(I)$]^a	0.0148
wR_2 [$I > 2\sigma(I)$]^b	0.0458
largest diff peak/hole (e/Å^3)	0.476/−0.390

$^aR_1 = \sum||F_o| - |F_c||/\sum|F_o|$. $^bwR_2 = [\sum[w(F_o^2 - F_c^2)^2]/\sum[w(F_o^2)^2]]^{1/2}$.

Table 2. Atomic Coordinates and Equivalent Isotropic Displacement Parameters (U_{eq}[a]) for $Sc_3Mn_3Al_7Si_5$

atom	site	x	y	z	U_{eq} (Å^2)
Sc	6*h*	0.20041(2)	0.40082(5)	1/4	0.0093(1)
Mn	6*g*	1/2	0	0	0.0082(1)
Al1	12*k*	0.16318(2)	0.32637(5)	0.57937(4)	0.0102(1)
Al2	2*b*	0	0	1/4	0.0127(2)
Si1	6*h*	0.55995(3)	0.11990(6)	1/4	0.0100(1)
Si2	4*f*	1/3	2/3	0.04029(6)	0.0089(1)

$^aU_{eq}$ is defined as one-third of the trace of the orthogonalized U_{ij} tensor.

Table 3. Important Interatomic Distances (Å) in $Sc_3Mn_3Al_7Si_5$

Sc−Si1 (2×)	2.8532(4)	Al2−Al1 (6×)	2.8241(4)
Sc−Si2 (2×)	2.7068(4)	Al2−Sc (3×)	2.8991(3)
Sc−Al1 (2×)	3.0402(4)	Mn−Si1 (2×)	2.4311(2)
Sc−Al1 (4×)	3.0881(3)	Mn−Si2 (2×)	2.4386(2)
Sc−Al2	2.8991(3)	Mn−Al1 (4×)	2.5410(2)
Sc−Mn (4×)	3.1674(1)	Mn−Sc (4×)	3.1674(1)
Al1−Mn (2×)	2.5410(2)	Si1−Mn (2×)	2.4311(2)
Al1−Si1 (2×)	2.6542(3)	Si1−Al1 (4×)	2.6542(3)
Al1−Si2	2.6907(4)	Si1−Sc (2×)	2.8532(4)
Al1−Al1 (2×)	2.7662(5)	Si2−Mn (3×)	2.4386(2)
Al1−Al2	2.8241(4)	Si2−Al1 (3×)	2.6907(4)
Al1−Sc (2×)	3.0402(4)	Si2−Sc (2×)	2.7068(4)

the assignments of Al and Si sites were based on their atomic sizes and electronegativities; that is, the smaller and more electronegative Si should have shorter distances between the more electropositive Mn and Sc.[24] Therefore, the 6*h* (0.55995 0.11990 1/4) and 4*f* sites are assigned to Si, and the 12*k* and 2*b* sites to Al (Table 2). These assignments resulted in reasonable distances between all the atoms. The occupancy of each atom site was also checked by freeing the site occupation factor (SOF) of an individual site while keeping the remaining parameters fixed. All of the SOFs remained close to unity. The resulting composition $Sc_3Mn_3Al_7Si_5$ was consistent with the composition determined from energy dispersive X-ray spectroscopy (EDS). While it is certain that Sc and Mn sites are fully occupied and without detectable site disorder, we cannot rule out the possibility that Al and Si may be disordered among all four sites, with the 6*h* and 4*f* sites more Si-rich and 12*k* and 2*b* sites more Al-rich.

Several bar-shaped crystals were crushed and ground into powder for a powder X-ray diffraction experiment, which was carried out on a Bruker D8 Advance diffractometer. The intensity data were collected

dx.doi.org/10.1021/ic501088t | Inorg. Chem. 2014, 53, 9115−9121

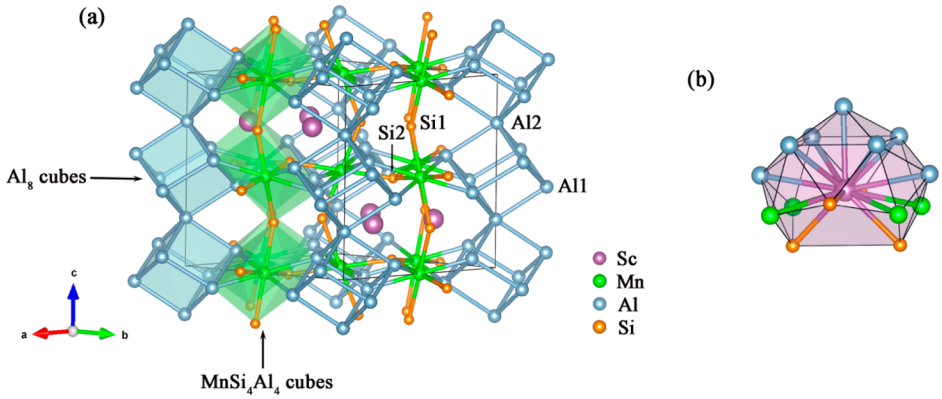

Figure 2. (a) Combined ball-and-stick and polyhedral representation of the crystal structure of $Sc_3Mn_3Al_7Si_5$, projected approximately along the [1 1 0] direction. The unit cell is outlined (black solid line). (b) The coordination environment of Sc.

with 2θ from 10° to 90° with an exposure time of 2 s. The collected patterns matched very well with the patterns simulated from single-crystal XRD data.

A ZEISS AURIGA 60 high-resolution focused ion beam and scanning electron microscope equipped with an Oxford Synergy X-MAX80 detector was used to take images of the crystals as well as for elemental analysis. The secondary electron (SE) and backscattered electron (BSE) images of a $Sc_3Mn_3Al_7Si_5$ crystal are displayed side by side in Figure 1, showing that the crystal is compositionally homogeneous. EDS was used to independently confirm the composition of the new compound. Spectra were collected on multiple crystals, and the results were then averaged. The determined composition, $Sc_{3.00(5)}Mn_{2.97(6)}Al_{7.08(5)}Si_{5.02(16)}$, agrees well with the refined formula from single-crystal X-ray diffraction. The Ga compositions in all doped samples were also independently determined by EDS, which results were in good agreement with the XRD refinements (details provided as Supporting Information).

Magnetic susceptibility measurements were conducted on single crystals using a Quantum Design magnetic property measurement system (MPMS) in the temperature range 1.8−300 K and for a magnetic field of 0.1 T, which was aligned parallel and perpendicular to the *c*-axis. Electrical resistivity measurements were carried out using a Quantum Design physical property measurement system (PPMS) on polished bar-shaped samples with a dc excitation current of 1 mA. Low resistance electrical contacts were made using silver-filled epoxy. The heat capacity C_p was also measured using the PPMS for temperatures ranging from 1.8 to 275 K.

RESULTS AND DISCUSSION

A new intermetallic compound, $Sc_3Mn_3Al_7Si_5$, has been synthesized from reactive aluminum flux. It crystallizes with a hexagonal structure in space group $P6_3/mmc$ (no. 194, Pearson symbol *hP*36), with six unique crystallographic sites in an asymmetric unit: Sc (6*h*), Mn (6*g*), Al1 (12*k*), Al2 (2*b*), Si1 (6*h*), and Si2 (4*f*). Several other intermetallic compounds are also reported to adopt the same structure, e.g., $Sc_3Ni_{11}Si_4$,[25] $Dy_3Cu_{11}Si_4$,[26] and the nonstoichiometric $Y_{21.04}Mg_{18.28}Zn_{60.68}$,[27] suggesting that this structure is capable of hosting a variety of valence electron concentrations. Five Ga-doped compounds, $Sc_3Mn_3(Al_{0.975}Ga_{0.025(1)})_7Si_5$, $Sc_3Mn_3(Al_{0.938}Ga_{0.062(1)})_7Si_5$, $Sc_3Mn_3(Al_{0.907}Ga_{0.093(1)})_7Si_5$, $Sc_3Mn_3(Al_{0.844}Ga_{0.156(1)})_7Si_5$, and $Sc_3Mn_3(Al_{0.810}Ga_{0.190(2)})_7Si_5$, were also obtained, and their structures were established by single-crystal X-ray diffraction as well. We will first report the crystal structure, chemical bonding, and physical properties of the parent compound $Sc_3Mn_3Al_7Si_5$, followed by the structural characteristics and magnetic properties of the doped samples.

The crystal structure of $Sc_3Mn_3Al_7Si_5$ is shown in Figure 2, projected approximately along the [1 1 0] direction. As seen from the figure, Mn atoms are surrounded by four Si atoms arranged in a square, and these squares are further connected by sharing Si1 along the *c*-axis and by sharing Si2 within the *ab*-plane, where Si1 is 2-bonded and Si2 is 3-bonded to Mn. The Mn−Si1 and Mn−Si2 distances, 2.4311(2) and 2.4386(2) Å, respectively, are in good agreement with the sum of Pauling's single-bond radii of Mn and Si,[24] indicating strong hybridization between Mn and Si. The distances are also comparable with those in binary and ternary manganese silicides such as Mn_5Si_3,[28] Mn_4Si_7,[28] $Sc_4Mn_4Si_7$,[29] and $Ti_2Mn_4Si_5$.[30] Four Al atoms are also found to be close to Mn with a Mn−Al distance of 2.5410(2) Å, which compares well with the distances in Mn_3Al, Mn_3Al_{10}, and $MnAl_6$.[28] Including the closest Al atoms, the Mn coordination is augmented as a distorted cube. Such a cubic coordination environment has also been noted in other intermetallic compounds such as CoMnSb[31] and $MnGa_4$.[32] On the other hand, Al1 and Al2 form Al_8 cubes, in which Al2 atoms are shared between neighboring cubes; hence they are fused diagonally along the *c*-axis. The distances between Al atoms, 2.7662(5) and 2.8241(4) Å, are slightly smaller than the distance in Al metal, 2.864 Å,[28] suggesting a metallic bonding character of the Al−Al contacts in the title compound. Relatively short Al−Si distances are also found between Al1 and Si (Table 3); these contacts could be considered as at least partial bonding, if not full. By sharing the common Al−Al edges, the $MnSi_4Al_4$ and Al_8 cubes are interconnected, forming a complex three-dimensional structural network.

Sc atoms occupy the voids created by the $MnSi_4Al_4$ and Al_8 cubes. The void or the cage-like coordination environment of Sc could be described as a 15-vertex polyhedron, which is composed of 20 triangular and two pentagonal faces (Figure 2b). With Sc atoms being the most electropositive element in the structure (Pauling scale: χ_{Sc} = 1.36, χ_{Mn} = 1.55, χ_{Al} = 1.61, χ_{Si} = 1.90[24]), it is assumed that the interactions between Sc and the other elements are more ionic (less covalent) than the interactions among Mn/Al/Si. Indeed, it has been reported by DFT calculations that for transition metal monosilicides *TM*Si, the larger the electronegativity of the transition metal, the higher the covalent character in the *TM*−Si bonds.[33] The Sc−Si, Sc−Al, and Sc−Mn distances (Table 3) compare well with the distances in their binary phases with high Sc coordination numbers, such as in $ScMn_2$,[34] ScAl,[35] and $ScSi_2$.[36]

The most prominent feature of the structure is that Mn, as the only magnetic element, forms corner-shared triangular nets,

dx.doi.org/10.1021/ic501088t | *Inorg. Chem.* 2014, 53, 9115−9121

i.e., the Kagome nets (Figure 3). The Mn−Mn distance within the Kagome plane is found to be 4.1759(1) Å, while these

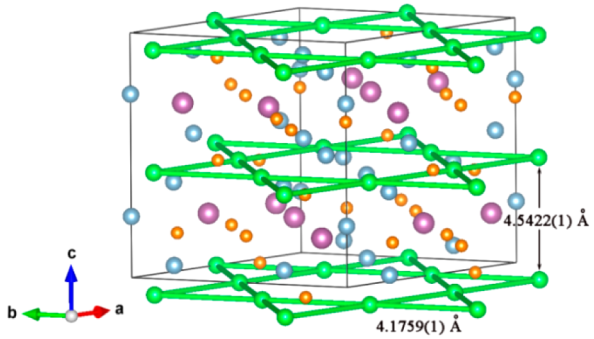

Figure 3. View of the crystal along the *c*-axis, in which the Kagome nets of Mn (green atoms) are highlighted.

planes are separated from each other by Sc/Al/Si slabs at a distance of 4.5422(1) Å. The Mn−Mn distance within the Kagome plane is more than 50% longer than those in the Mn metal,[28] and it is also significantly longer than those in the above-mentioned RMn_6X_6 compounds, for example, 2.605 Å in YMn_6Ge_6,[37] 2.745 Å in $LiMn_6Sn_6$[38] and 2.758 Å in $MgMn_6Sn_6$.[39] Such a long Mn−Mn distance in $Sc_3Mn_3Al_7Si_5$ most likely makes direct overlap of Mn 3d orbitals unimportant for determining the electronic structure.

Following the descriptions of the structure and bonding, a few aspects of the properties of $Sc_3Mn_3Al_7Si_5$ could be expected. First, metallic bonding is most likely dominant in $Sc_3Mn_3Al_7Si_5$ since the high coordination numbers of all atoms would not be satisfied if only localized bonds were considered. From this point of view, we expect $Sc_3Mn_3Al_7Si_5$ to be a metal. Also, with complex bonding and hybridization among atoms extending three dimensionally, it is possible that the anisotropic nature apparent in the crystal structure may not be reflected in the physical properties of this system. Last, but probably most interestingly, $Sc_3Mn_3Al_7Si_5$ should feature frustrated magnetism, as expected from the Mn Kagome net. Although direct exchange of Mn is probably not plausible due to the large Mn−Mn distance, magnetic coupling between Mn d electrons and the conduction band is likely to play a significant role in magnetism.

The temperature dependence of the electrical resistivity ρ of $Sc_3Mn_3Al_7Si_5$, measured with the current flowing along the *c*-axis is shown in Figure 4. The resistivity is predominantly metallic, decreasing from a room-temperature value of 250 $\mu\Omega$·cm to a minimum value of ∼120 $\mu\Omega$·cm at ∼30 K. An upturn in resistivity is observed below 30 K. We have measured resistivity of crystals from two different batches, and the temperatures of the minimum and the upturn magnitude are sample independent.

Figure 5 shows the temperature dependence of the magnetic susceptibility $\chi(T)$, measured in a 0.1 T magnetic field aligned both parallel and perpendicular to the *c*-axis. The curves are almost the same, revealing very weak anisotropy and strong temperature dependencies for both field directions. The susceptibility is featureless, with no indication of a magnetic phase transition for temperatures as low as 1.8 K. We were able to fit the 50−300 K temperature region to the modified Curie−Weiss law:

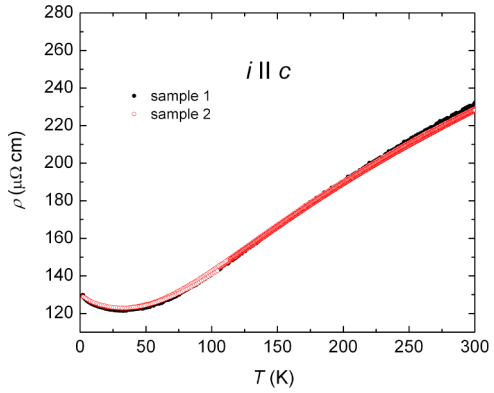

Figure 4. Temperature dependence of electrical resistivity of $Sc_3Mn_3Al_7Si_5$.

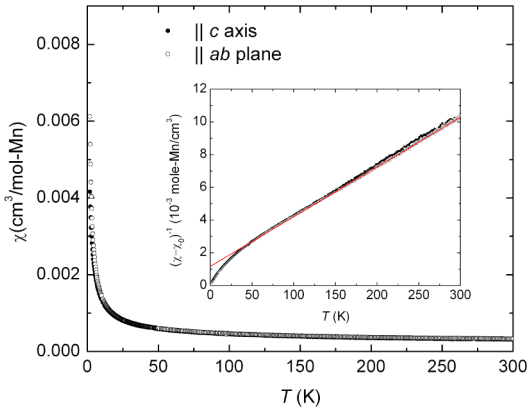

Figure 5. Magnetic susceptibility of $Sc_3Mn_3Al_7Si_5$ measured with a 0.1 T field parallel (filled circles) and perpendicular (open circles) to the crystallographic *c*-axis. The inset shows the fits to a Curie−Weiss expression for the temperature-dependent part of the inverse susceptibility $(\chi-\chi_0)^{-1}$.

$$\chi(T) = \frac{N_A g^2 \mu_B^2 J(J+1)}{3k_B(T-\theta_{CW})} + \chi_0 \quad (1)$$

where θ_{CW}, J, g, k_B, and χ_0 are respectively the Weiss temperature, the angular momentum of the Mn moments, the Landé *g*-factor, the Boltzmann constant, and a temperature-independent contribution to the susceptibility. A least-squares fit, performed above 50 K (inset in Figure 5), yielded an effective moment $\mu_{eff} = g\mu_B(J(J+1))^{0.5} = 0.51(1)\mu_B$/Mn in both directions, $\theta_{CW} = -38(1)$ K and $\chi_0 = 23.5(1) \times 10^{-5}$ emu/mol Mn along the *c*-axis, and $\theta_{CW} = -39(1)$ K and $\chi_0 = 21.7(1) \times 10^{-5}$ emu/mol Mn for a magnetic field perpendicular to the *c*-axis. All these quantities are very similar for both field directions, suggesting that magnetic anisotropy is minimal in this system, consistent with the complex 3D bonding in this compound. The strongly reduced values of the effective moments are consistent with a small polarized electron density, establishing the itinerant character of the magnetism in this system. We have measured magnetic susceptibility of crystals from different batches, and the values of effective moments and characteristic θ_{CW} temperatures agreed within 5% with the aforementioned values. As our single crystals are of high quality and our structural analysis excludes the presence of Mn ions outside the Kagome planes, it is likely that the observed magnetic properties are intrinsic. Taking into consideration that the nearest Mn−Mn distances are very large, and so direct Mn

dx.doi.org/10.1021/ic501088t | Inorg. Chem. 2014, 53, 9115−9121

3d−Mn 3d hybridization should be insignificant, we infer that in $Sc_3Mn_3Al_7Si_5$ hybridization between Mn 3d and ligands, most likely the s and p states of Al and Si, should play a dominant role in the magnetic properties. This assumption is consistent with the accepted picture of magnetism in Mn−Si binary systems. Here, the Mn magnetism is suppressed with increasing Si content, where Mn-rich Mn_3Si,[40] Mn_5Si_3,[41] and MnSi[42] all order magnetically, whereas silicon-rich $Mn_{11}Si_{19}$ and Mn_4Si_7[43] do not. $Sc_3Mn_3Al_7Si_5$, with highly coordinated Mn with Si and Al ions, seems to correspond well to the latter two silicides.

A special comment should be made regarding the values of θ_{CW}. According to the mean field theory, $|\theta_{CW}|$ sets the energy scale for the onset of long-range magnetic interactions.[44] The relatively high Weiss temperature (about −40 K) and the absence of order for $Sc_3Mn_3Al_7Si_5$ down to 1.8 K may be a sign of a spin liquid state in this metal that the Kagome net suggests. The measure of frustration is the f parameter, defined as $f = (|\theta_{CW}|)/(T_{ord})$, where T_{ord} stands for the ordering temperature. An f value bigger than 10 usually indicates strong magnetic frustration in the system.[3] In $Sc_3Mn_3Al_7Si_5$, f is higher than 22 (taking the ordering temperature to be no higher than 1.8 K); this renders $Sc_3Mn_3Al_7Si_5$ as a strong frustrated material.

Figure 6 shows the temperature dependence of the heat capacity ratio C_p/T. As shown from the figure, no anomaly is

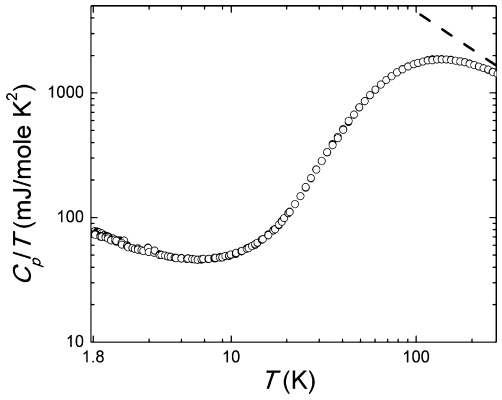

Figure 6. $Sc_3Mn_3Al_7Si_5$ C_p/T ratio versus temperature. The dotted line represents the Dulong−Petit limit.

found that would point to the existence of an electronic, magnetic, or structural phase transition over the temperature range 1.8−275 K. The dotted line indicates the Dulong−Petit limit $C_{DP}/T = 3Rn/T$, where R is the gas constant and n is the number of atoms per formula unit. At 275 K, the total heat capacity reaches 389 J/mol-K, which is only 86% of the Dulong−Petit limit, indicating a relatively high Debye temperature of the compound. Very intriguing behavior is noted in C_p/T for the low-temperature range. At $T < 10$ K, an additional contribution to C_p emerges, leading to the divergence of C_p/T and a relatively high Sommerfeld coefficient of 80 mJ/mol-K^2 at 1.8 K, suggesting strong electronic correlations.

The anomalous divergencies in both specific heat and magnetic susceptibility indicate that the system is on the verge of some kind of magnetic/electronic phase transition that occurs below 1.8K. Two types of T = 0 instabilities are commonly discussed. In the first, magnetic order is suppressed to T=0 by increasing the hybridization between the magnetic moment and the conduction electrons, leading to the vanishing of the moment. This usually occurs in the *f*-electron based compounds via the Kondo effect. A second scenario is that the magnetic moments are robust, but the magnetic order is suppressed by quantum fluctuations, introduced via low dimensionality or by competing interactions arising in a frustrated lattice. Considering that the Mn moments lie on a frustrated Kagome net, the second scenario seems to be more plausible, although the possibility of moment compensation cannot yet be ruled out. In the presence of strong magnetic frustration, we speculate that the moments may potentially form a highly degenerate magnetic ground state at $T = 0$, resulting in a quantum spin liquid. Future experiments at lower temperatures will be needed to explore this possibility.

Moving onto the five Ga-doped compounds, as we previously pointed out, all of them adopt the same crystal structure as $Sc_3Mn_3Al_7Si_5$. Two interesting observations deserve discussion. First, according to single-crystal XRD refinements, Ga substitutes only for the Al atoms, leaving the Mn Kagome layers intact from doping, which is understandable since Ga and Al are from the same element group. The Mn−Mn distances are only slightly shorter in the doped samples, decreasing from 4.1759(1) Å in $Sc_3Mn_3Al_7Si_5$ to 4.1564(1) Å in $Sc_3Mn_3(Al_{0.810}Ga_{0.190(2)})_7Si_5$. Second, as seen from Figure 7,

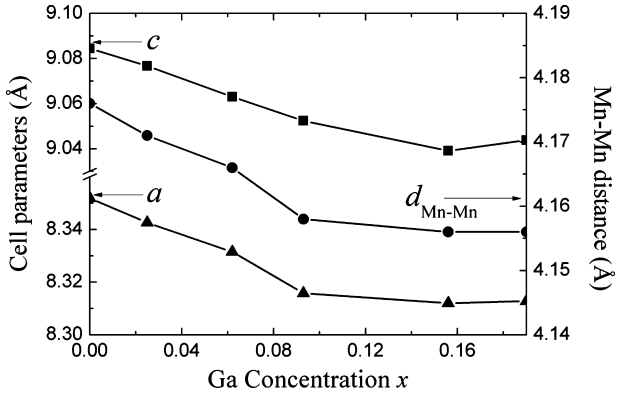

Figure 7. Dependence of the cell parameters a and c, as well as the Mn−Mn distances on the Ga concentrations in $Sc_3Mn_3(Al_{1-x}Ga_x)_7Si_5$.

d_{Mn-Mn}, or in general the cell parameters a and c, do not decrease linearly for the whole doping range. While a and c decrease linearly as the Ga doping concentration increases up to 9.3%, they remain almost unchanged as Ga% further increases. Looking into the details of the site occupancy reveals a plausible explanation to this anomaly. From XRD refinements (see Table S2), Ga has a clear preference for the Al2(2*b*) site, as it occupies only the Al2(2*b*) site as its doping concentration increase up to 9.3%. With higher Ga doping, it starts to occupy both Al2(2*b*) and Al1(12*k*) sites, with 88.1% Ga occupancy at the 2*b* site and only 3.5% at the 12*k* site for $Sc_3Mn_3(Al_{0.844}Ga_{0.156(1)})_7Si_5$, and 93.6% Ga occupancy at the 2*b* site and 6.5% at the 12*k* site for $Sc_3Mn_3(Al_{0.810}Ga_{0.190(2)})_7Si_5$. We believe that the onset of the Ga substitution at the Al1 site (which is different from the Al2 site) has caused the deviation of the cell parameters from linear decrease when Ga doping is above 10%, since XRD refinements clearly suggest the concurrence of them. Similar behaviors have been observed in Garnet structure compounds $Y_3Al_{5-x}Ga_xO_{12}$ and $Y_3Fe_{5-x}Ga_xO_{12}$ ($0 \le x \le 5$), where deviation from the Vegard's law is also related to the site preference of the dopants.[45,46]

The magnetic susceptibilities of the Ga-doped single crystals have also been measured along their crystallographic *c*

dx.doi.org/10.1021/ic501088t | *Inorg. Chem.* 2014, 53, 9115−9121

direction. As seen from Figure 8, the susceptibilities of the two lowest doped samples (x = 0.025 and 0.062) remain almost the same as the parent compound, i.e., the values are very close for the whole measured temperature range and no anomaly is observed down to 1.8 K. On the other hand, the susceptibilities of the higher doped samples are enhanced. Fitting the data from 50 to 300 K to eq 1, we obtain effective moments of 0.54, 0.69, and 0.79 μ_B/Mn for $Sc_3Mn_3(Al_{0.907}Ga_{0.093(1)})_7Si_5$, $Sc_3Mn_3(Al_{0.844}Ga_{0.156(1)})_7Si_5$, and $Sc_3Mn_3(Al_{0.810}Ga_{0.190(2)})_7Si_5$, respectively. Compared with the moment of 0.51(1)μ_B/Mn for the parent compound, the moments enhanced in the latter two samples are noteworthy. As we previously discussed, Mn 3d-ligand hybridization plays a dominant role in the magnetic property of $Sc_3Mn_3Al_7Si_5$. We speculate that the enhanced moment in the Ga-doped samples could be attributed to the weakening of Mn 3d-ligand hybridization, as Ga s and p states should lie further below the Fermi level due to its higher electronegativity than Al. Indeed, the enhancement of magnetic moments is found to be significant only in the two highest doped compounds, in which Ga also occupies the Al1($12k$) site, leading to direct overlap of Mn−Ga. Similar scenarios are found in the uranium compounds UX_3 and UTX (T = transition metal, X = triel/tetrel), where 5f-ligand hybridization is considered as the primary mechanism determining their magnetic properties.[47,48]

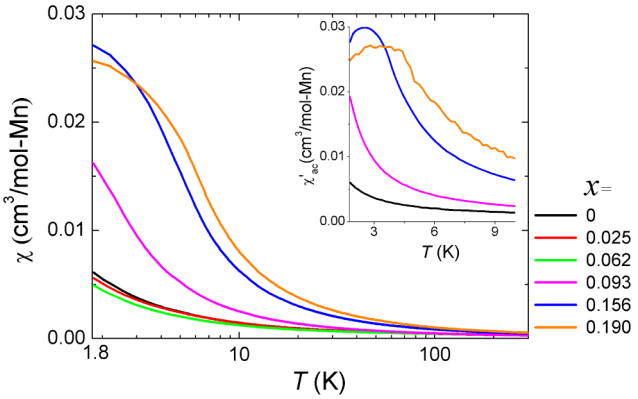

Figure 8. Direct current (dc) magnetic susceptibility of $Sc_3Mn_3(Al_{1-x}Ga_x)_7Si_5$ measured with a 0.1 T field parallel to the crystallographic c-axis. The inset shows ac susceptibility measured with a frequency of 17 Hz at zero dc field.

At the lowest temperature range it is noted that the χ-T curves for the two highest Ga-doped compounds start to saturate, indicating the possible onset of a magnetic phase transition. These anomalies are more clearly shown in the AC susceptibility measurements (Figure 8 inset), where peaks at ~2.5K are observed for $Sc_3Mn_3(Al_{0.844}Ga_{0.156(1)})_7Si_5$ and at ~3.6K for $Sc_3Mn_3(Al_{0.810}Ga_{0.190(2)})_7Si_5$. In the presence of strong geometrical frustration from the Kagome net, in combination with the chemical disorder introduced by the Ga doping, it is very plausible that these anomalies reflect a spin glass transition. The spin glass is a ground state that often occurs in systems with evident disorder, reflecting compromised order on very short length scales. Upon doping the Mn magnetic sublattice remains undisturbed and disorder is limited only to p metalloid site, suggesting that $Sc_3Mn_3(Al,Ga)_7Si_5$ may be classified as the nonmagnetic atom disorder (NMAD) spin glass.[49] We argue that the presence of the local magnetic order in doped samples is strong evidence of the intrinsic and frustrated character of magnetism in the parent compound.

CONCLUSIONS

We have synthesized high-quality single crystals of a new intermetallic compound $Sc_3Mn_3Al_7Si_5$ and its Ga-doped analogues $Sc_3Mn_3(Al,Ga)_7Si_5$. The crystal structures have been established by single-crystal X-ray diffraction, and the compositions have been confirmed with EDS measurements. $Sc_3Mn_3Al_7Si_5$ crystallizes in a hexagonal structure with the $Sc_3Ni_{11}Si_4$ type. Two types of cubic motifs, $MnSi_4Al_4$ and Al_8, are identified, and by sharing the common Al and Si atoms, they are condensed into a 3D network, creating voids that are occupied by Sc atoms. Intriguingly, we find that the Mn ions bear a small moment, and they form geometrically frustrated Kagome nets. No magnetic or other type of order is observed in $Sc_3Mn_3Al_7Si_5$ for temperatures as low as 1.8 K. A large Weiss temperature suggests that the moments are effectively coupled and may collectively fluctuate down to the lowest temperatures. The absence of magnetic order suggests that these interactions are frustrated and thus cannot lead to magnetic order. This material is definitively metallic, establishing it as a rare example of a metallic Kagome system, where the absence of static magnetic order may lead to the realization of a quantum spin liquid ground state. The presence of short-range order in Ga-doped samples is a direct evidence for the intrinsic character of magnetism in $Sc_3Mn_3Al_7Si_5$ and generic frustration within the Mn triangular plane.

ASSOCIATED CONTENT

Supporting Information

CIF file of $Sc_3Mn_3Al_7Si_5$; tables of crystallographic data of $Sc_3Mn_3(Al,Ga)_7Si_5$, including refinement parameters, atomic sites, and interatomic distances; table of the composition of the Ga-doped samples from EDS; figure of the frequency dependence of the ac magnetic susceptibility of $Sc_3Mn_3(Al_{0.844}Ga_{0.156(1)})_7Si_5$. This material is available free of charge via the Internet at http://pubs.acs.org.

AUTHOR INFORMATION

Corresponding Author

*E-mail: hua.he@stonybrook.edu.

Author Contributions

The manuscript was written through contributions of all authors. All authors have given approval to the final version of the manuscript.

Notes

The authors declare no competing financial interest.

ACKNOWLEDGMENTS

Work at Stony Brook University was carried out under the auspices of a Department of Defense National Security Science and Engineering Faculty Fellowship via Air Force Office of Scientific Research grant FA 9550-10-1-0191. H.H. acknowledges Mr. Chang Liu and Dr. Chaoying Ni for the EDS measurements at the W.M. Keck Electron Microscopy Facility at the University of Delaware.

REFERENCES

(1) Balents, L. *Nature* **2010**, *464*, 199−208.
(2) Greedan, J. E. *J. Mater. Chem.* **2001**, *11*, 37−53.
(3) Ramirez, A. P. *Annu. Rev. Mater. Sci.* **1994**, *24*, 453−480.

(4) Binder, K.; Young, A. P. *Rev. Mod. Phys.* **1986**, *58*, 801−976.
(5) Bramwell, S. T.; Gingras, M. J. P. *Science* **2001**, *294*, 1495−1501.
(6) Fazekas, P.; Anderson, P. W. *Philos. Mag.* **1974**, *30*, 423−440.
(7) Pauling, L. *J. Am. Chem. Soc.* **1935**, *57*, 2680−2684.
(8) Anderson, P. W. *Mater. Res. Bull.* **1973**, *8*, 153−160.
(9) Anderson, P. W. *Science* **1987**, *235*, 1196−1198.
(10) Miiller, W.; Christensen, M.; Khan, A.; Sharma, N.; Macquart, R. B.; Avdeev, M.; McIntyre, G. J.; Piltz, R. O.; Ling, C. D. *Chem. Mater.* **2011**, *23*, 1315−1322.
(11) Colman, R. H.; Sinclair, A.; Wills, A. S. *Chem. Mater.* **2011**, *23*, 1811−1817.
(12) Lee, S. H.; Kikuchi, H.; Qiu, Y.; Lake, B.; Huang, Q.; Habicht, K.; Kiefer, K. *Nat. Mater.* **2007**, *6*, 853−857.
(13) Han, T. H.; Helton, J. S.; Chu, S. Y.; Nocera, D. G.; Rodriguez-Rivera, J. A.; Broholm, C.; Lee, Y. S. *Nature* **2012**, *492*, 406−410.
(14) Baranov, N. V.; Gerasimov, E. G.; Mushnikov, N. V. *Phys. Met. Metallogr.* **2011**, *112*, 711−744.
(15) Kishimoto, Y.; Kawasaki, Y.; Ohno, T.; Gupta, L. C.; Ghosh, G. *J. Phys. Soc. Jpn.* **2004**, *73*, 190−193.
(16) Li, S.; Zeng, B.; Wan, X.; Tao, J.; Han, F.; Yang, H.; Wang, Z.; Wen, H.-H. *Phys. Rev. B* **2011**, *84*, 045111-1−045111-6.
(17) Stewart, J. R.; Rainford, B. D.; Eccleston, R. S.; Cywinski, R. *Phys. Rev. Lett.* **2002**, *89*, 214527−1−214527−6.
(18) Lacroix, C.; Canals, B. *J. Magn. Magn. Mater.* **1999**, *196*−*197*, 622−624.
(19) Okamoto, Y.; Shimizu, T.; Yamaura, J.-I.; Kiuchi, Y.; Hiroi, Z. *J. Phys. Soc. Jpn.* **2010**, *79*, 093712-1−093712-4.
(20) Lacroix, C. *Can. J. Phys.* **2001**, *79*, 1469−1473.
(21) Burdin, S.; Grempel, D. R.; Georges, A. *Phys. Rev. B* **2002**, *66*, 045111-1−045111-6.
(22) Ferro, R.; Saccone, A.; Delfino, S.; Maccio, D.; Giovannini, M. *Powder Metall. Met. Ceram.* **1997**, *36*, 117−127.
(23) Sheldrick, G. M. *SHELXTL*; University of Göttingen,: Göttingen, Germany, 2001.
(24) Pauling, L. *The Nature of the Chemical Bond*; Cornell University Press: Ithaca, NY, 1960.
(25) Kotur, B. Y.; Sikiritsa, M.; Bodak, O. I.; Gladyshevsky, E. I. *Kristallografiya* **1983**, *28*, 658−661.
(26) Morozkin, A. V.; Manfrinetti, P. *J. Alloys Compd.* **2007**, *437*, 165−168.
(27) Deng, D. W.; Kuo, K. H.; Luo, Z. P.; Miller, D. J.; Kramer, M. J.; Dennis, K. W. *J. Alloys Compd.* **2004**, *373*, 156−160.
(28) Villars, P. *Pearson's Handbook of Crystallographic Data for Intermetallic Phases*, desktop ed.; ASM International: Materials Park, OH, 1997.
(29) Kotur, B. Y.; Bodak, O. I.; Kotur, O. Y. *Dopov. Akad. Nauk Ukr. Rsr Ser. A* **1980**, 80−83.
(30) Steinmetz, J.; Venturini, G.; Roques, B.; Engel, N.; Chabot, B.; Parthe, E. *Acta Crystallogr.* **1982**, *B38*, 2103−2108.
(31) Szytula, A.; Szelag, J.; Todorovi, J.; Wanic, A.; Dimitrij, Z.; Kolodzie, A. *Phys. Status Solidi A* **1972**, *9*, 97−103.
(32) Tillard, M.; Belin, C. *Intermetallics* **2012**, *29*, 147−154.
(33) Wu, Z. J.; Su, Z. M. *J. Chem. Phys.* **2006**, *124*, 184306−1−184306−15.
(34) Wu, M. M.; Tang, B. Y.; Peng, L. M.; Ding, W. J. *Phys. B: Condens. Matter* **2010**, *405*, 4812−4817.
(35) Schob, O.; Parthe, E. *Acta Crystallogr.* **1965**, *19*, 214−224.
(36) Kotroczo, V.; McColm, I. J. *J. Alloys Compd.* **1994**, *203*, 259−265.
(37) Venturini, G.; Welter, R.; Malaman, B.; Ressouche, E. *J. Alloys Compd.* **1993**, *200*, 51−57.
(38) Mazet, T.; Ihou-Mouko, H.; Marêché, J.; Malaman, B. *Eur. Phys. J. B* **2006**, *51*, 173−180.
(39) Mazet, T.; Venturini, G.; Welter, R.; Malaman, B. *J. Alloys Compd.* **1998**, *264*, 71−75.
(40) Tomiyoshi, S.; Watanabe, H. *J. Phys. Soc. Jpn.* **1975**, *39*, 295−302.
(41) Menshikov, A. Z.; Vokhmyanin, A. P.; Dorofeev, Y. A. *Phys. Status Solidi B* **1990**, *158*, 319−328.
(42) Thessieu, C.; Flouquet, J.; Lapertot, G.; Stepanov, A.; Jaccard, D. *Solid State Commun.* **1995**, *95*, 707−712.
(43) Hammura, K.; Udono, H.; Ohsugi, I. J.; Aono, T.; De Ranieri, E. *Thin Solid Films* **2011**, *519*, 8516−8519.
(44) Smart, J. S. *Effective Field Theories of Magnetism*; Saunders: Philadelphia, PA, 1966.
(45) Nakatsuka, A.; Yoshiasa, A.; Takeno, S. *Acta Crystallogr.* **1995**, *B51*, 737−745.
(46) Nakatsuka, A.; Yoshiasa, A.; Takamitsu, Y. *Acta Crystallogr.* **1999**, *B55*, 266−272.
(47) Strange, P. *J. Phys. F: Met. Phys.* **1986**, *16*, 1515−1524.
(48) Koelling, D. D.; Dunlap, B. D.; Crabtree, G. W. *Phys. Rev. B* **1985**, *31*, 4966−4971.
(49) Gschneidner, K. A., Jr.; Tang, J.; Dhar, S. K.; Goldman, A. *Phys. B: Condens. Matter* **1990**, *163*, 507−510.